One- and two-photon Compton scattering in strong magnetic fields

R. W. Bussard
Space Science Laboratory, NASA Marshall Space Flight Center, Alabama 35812
and Astronomy Department, Pennsylvania State University, University Park, Pennsylvania 16802

S. B. Alexander
Astronomy Department, Pennsylvania State University, University Park, Pennsylvania 16802

P. Mészáros
Physics Department, Pennsylvania State University, University Park, Pennsylvania 16802
(Received 11 February 1986)

We calculate the Compton scattering cross section in a very strong magnetic field ($B \sim 10^{12}$ G), such as encountered in pulsars, for arbitrary photon and electron energies. We include the effect of the vacuum polarization in the weak-field limit ($B \ll m^2c^3/\hbar e$), as well as the plasma polarizability. We include explicitly radiative transitions between any pair of Landau levels, and include also two-photon scattering. The latter process, due to the presence of the cyclotron resonance, becomes comparable to nonresonant one-photon scattering when excited final states are allowed, and acts as a source of photons which is more important than bremsstrahlung at low plasma densities. The treatment is based on the relativistic S matrix, and the cross sections are averaged over a relativistic Maxwellian electron distribution. The results are compared with previous nonrelativistic calculations, and it is found that even for temperatures as low as 10 keV there are significant effects that are peculiar to the relativistic treatment.

I. INTRODUCTION

The astrophysics of strongly magnetized neutron stars has given impetus to a number of calculations involving the application of quantum electrodynamics to situations where the external field can no longer be treated as a perturbation. The pulsing x-ray binary stellar systems, such as Hercules X-1, constitute one class of neutron-star sources where the magnetic field strengths are inferred to be of the order of 10^{12} G. The cyclotron energy levels in such a field have a typical separation given by $E = 11.6(B/10^{12}\ \text{G})$ keV. Furthermore, the observed luminosity and spectra of such objects imply typical densities of order 10^{20}cm^{-3} and electron energies of order 10 keV or more (for a review of the observations, see Joss and Rappaport;[1] theoretical considerations have recently been reviewed by Mészáros[2]). For these conditions, a detailed interpretation of the radiation requires a knowledge of both emission and scattering mechanisms by fast, strongly magnetized electrons.

The first studies of radiation processes in a strong field were carried out in the nonrelativistic limit (Canuto, Lodenquai, and Ruderman,[3] Ventura,[4] Mészáros and Ventura,[5] etc.). From these studies, it was realized that the charged-particle collisional rates are inadequate to populate excited cyclotron levels; thus, the electron cyclotron energy-level distribution must be completely determined by the radiation density at the cyclotron frequency (and overtones). In such a situation, the absorption and emission of cyclotron radiation can be treated as a resonance in the scattering process, since essentially every radiative excitation is followed by a radiative deexcitation. Daugherty and Ventura[6] carried out a fully relativistic calculation of the absorption rate for cyclotron photons, and Herold[7] presented the differential scattering rates in the relativistic case, but with the electron confined to the magnetic ground level in both the initial and final states. The inclusion of relativistic effects was necessary to adequately describe line profiles and include the contributions from higher harmonics and spin-flip transitions in the sum over intermediate electron states.

In this paper, we present a detailed study of the photon-electron differential scattering rates in a strong magnetic field, using the covariant S-matrix formulation. In Sec. II general formulas for the rates are given for transitions between any levels for arbitrary photon polarization. These expressions show a typical general structure, in that they consist of products of matrix elements, one between the final and intermediate states and one between the intermediate and initial states. These products are then summed over the intermediate state with the inclusion of the appropriate energy denominator arising from the electron propagator. In Sec. III we show the results of numerical evaluations of the formulas for several cases likely to apply to the pulsing x-ray binaries. One particularly important result that comes from relaxing the assumption that the electron final state be the ground level is the existence of a resonance in the process analogous to double Compton scattering. In fact, this process is very likely the dominant source of photons for the parameters typical of accreting neutron stars. A preliminary discussion of the process and its implications has been given elsewhere (Bussard, Mészáros, and Alexander;[8] see also Kirk and Melrose[9]). Finally, in Sec. IV, we discuss the results and indicate their usefulness for various applications.

II. SCATTERING RATES

First, we describe the expressions used to obtain the scattering rates presented below. We have derived these formulas in the fully relativistic S-matrix representation, as, for example, in Bjorken and Drell,[10] and the calculations are outlined in the Appendix. The results can be written as

$$w_{j',s';j,s}(\mathbf{k}',\hat{\boldsymbol{\epsilon}}';\mathbf{k},\hat{\boldsymbol{\epsilon}},\mathbf{p})=\frac{1}{4}\frac{{r_0}^2}{\omega\omega'}\delta(\omega'-\omega+E'-E)\frac{m^2}{EE'}(E+m)(E'+m)\left|\sum_{j''}(a_{j''}e^{ij''(\phi'-\phi)}+b_{j''}e^{2i\Lambda-ij''(\phi'-\phi)})\right|^2 , \tag{1}$$

where $w_{j',s';j,s}(\mathbf{k}',\hat{\boldsymbol{\epsilon}}';\mathbf{k},\hat{\boldsymbol{\epsilon}},\mathbf{p})$ is the rate, j, s, and p refer to the electron magnetic quantum number, spin, and parallel momentum, $\mathbf{k}$ and $\hat{\boldsymbol{\epsilon}}$ are the photon wave vector and polarization vector, r_0 is the classical electron radius, m is the electron mass, ω is the photon frequency, and E refers to the electron energy. The primes refer to the final state, and units where $\hbar=c=1$ are used throughout. The δ function clearly expresses conservation of energy. The quantity within the vertical bars is a summation over intermediate electron states, in which the ϕ's are the azimuthal angles of the photons in the plane perpendicular to the field, and the a's, b's, and Λ are defined as (see the Appendix)

$$a_{j''}=\frac{E''+m}{2E''}\sum_{s'',\lambda''}\frac{[\hat{\boldsymbol{\epsilon}}'^*\cdot\mathbf{G}^{(\lambda'')}_{fq''}(-\mathbf{k}'_\perp)]\{[\mathbf{G}^{(\lambda'')}_{iq''}(-\mathbf{k}_\perp)]^*\cdot\hat{\boldsymbol{\epsilon}}\}}{E+\omega-\lambda''E''}\bigg|_{p''=p+k_{||}},$$

$$b_{j''}=\frac{E''+m}{2E''}\sum_{s'',\lambda''}\frac{[\hat{\boldsymbol{\epsilon}}'^*\cdot\mathbf{G}^{(\lambda'')}_{q''i}(-\mathbf{k}'_\perp)]\{[\mathbf{G}^{(\lambda'')}_{q''f}(-\mathbf{k}_\perp)]^*\cdot\hat{\boldsymbol{\epsilon}}\}}{E-\omega'-\lambda''E''}\bigg|_{p''=p-k'_{||}}, \tag{2}$$

$$\Lambda=\tfrac{1}{2}(j+j')(\phi'-\phi)+(\xi\xi')^{1/2}\sin(\phi'-\phi) ,$$

where s'' is the intermediate-state spin and λ'' the sign of the energy. In these equations, the energies are given by

$$E=(m^2+p^2+2m\omega_c j)^{1/2} , \tag{3}$$

and similarly for the primed and double primed terms, where ω_c is the classical cyclotron frequency. The G vectors arise from the matrix-element integrations and are discussed in the Appendix, while the energy denominators come from the electron propagators in the usual way. in Λ, the quantity ξ is given by $\hbar{k_\perp}^2/(2m\omega_c)$.

In the cases to which we wish to apply our calculations, we expect the densities to be low enough that the collisional excitation rates of magnetic states above the ground level are quite small compared to the radiative deexcitation rates, implying that the electrons spend essentially all their time in the ground state (Canuto and Ventura,[11] Bussard[12]). Thus, in what follows, we consider only cases where the initial electron has $j=0$. We note that Herold[7] has obtained the rate for the situation where both electron states are the ground state, and our expression agrees under that condition. However, we have generalized the calculation to include cases where the electron is left in an excited state after the scattering. This effect has important consequences for the production of radiation in the pulsing x-ray binaries (Bussard, Mészáros, and Alexander,[8] Kirk and Melrose[9]).

We can further simplify the scattering rate if we assume azimuthal symmetry. Integrating Eq. (1) over the final photon azimuth and averaging over the initial yields

$$w_{j's';j,s}(\omega',\mu',\hat{\boldsymbol{\epsilon}}';\omega,\mu,\hat{\boldsymbol{\epsilon}})=\frac{\pi}{2}{r_0}^2\frac{\omega'}{\omega}\delta(\omega'-\omega+E'-E)\frac{m^2}{EE'}(E+m)(E'+m)$$
$$\times\sum_{j''}\left[|a_{j''}|^2+|b_{j''}|^2+2\sum_{j_3}J_{j''+j_3-j'-j}(2\sqrt{\xi\xi'})\mathrm{Re}(a_{j''}b^*_{j_3})\right] , \tag{4}$$

where, in addition, we have converted from a rate differential in the three-dimensional wave vector to one differential in frequency and direction cosine μ (taken with respect to the field direction). In Eq. (4), the origin of the squares of a and b is evident, and the term involving the Bessel functions arises from the cross product of the a and b terms with the form of Λ taken into account. Finally, we use the δ function in an integration over the electron parallel momentum distribution, which is taken to be a relativistic thermal population, or

$$f(p)=\left[2mK_1\left[\frac{m}{T}\right]\right]^{-1}\exp\left[-\frac{E}{T}\right] , \tag{5}$$

where T is the electron temperature parallel to the field and K_1 denotes the modified Bessel function of the second kind. In performing this integration, one finds that for a given initial and final photon, there exist two electron momenta that satisfy conservation of energy and parallel momentum, which we denote $p_\pm$, given by

$$p_{\pm}=\frac{k'_{\parallel}-k_{\parallel}}{2q}[q+2m\omega_c(j'-j)]\pm\frac{\omega'-\omega}{2q}\{[q+2m\omega_c(j'-j)]^2+4q(m^2+2m\omega_c j)\}^{1/2}\,, \tag{6}$$

where $q=(k'_{\parallel}-k_{\parallel})^2-(\omega'-\omega)^2$. The resulting expression for the scattering rate becomes

$$w(\omega',\mu',\hat{\epsilon}';\omega,\mu,\hat{\epsilon})=\pi r_0{}^2\frac{\omega'}{\omega}\sum_{j',s'}\sum_{\pm}f(p_{\pm})\frac{m^2(E+m)(E'+m)}{[(q+2m\omega_c j')^2+4qm^2]^{1/2}}$$
$$\times\sum_{j''}\left[|a_{j''}|^2+|b_{j''}|^2+2\sum_{j_3}J_{j''+j_3-j-j'}(2\sqrt{\xi\xi'})\mathrm{Re}(a_{j''}b^*_{j_3})\right]. \tag{7}$$

For the purposes of this work, we have used the results of Bussard, Lamb, and Pakey[13] for the normal-mode eigenvectors in a thermal plasma. We merely note that the calculation is based on that of Pavlov, Shibanov, and Yakovlev,[14] generalized to the fully relativistic case. It includes both the effects of the polarizability due to the plasma electrons and the vacuum polarizability in the limit where $B/B_{\rm cr}=B\hbar e/m^2c^3=B/(4.412\times10^{13}\mathrm{G})\ll1$.

III. RESULTS

A. Differential scattering cross sections

The scattering rate derived in Sec. II was used to calculate differential cross sections for various incident photon frequencies and angles. In all cases, we used conditions believed to be typical of the free-fall atmosphere of an accreting x-ray pulsar: cyclotron energy $\hbar\omega_c=38$ keV; electron temperature kT=10 keV; plasma density $\rho=1.67\times10^{-2}$ g/cm^3, e.g., Ref. 2. The summations over final electron magnetic quantum number j' in Eq. (7) were included up to $j'=3$ while the summations over intermediate states extended to $j''=4$. Thus the cross sections should be considered accurate up to and including the second harmonic. In order to see the differences that would arise if one neglected relativistic effects, we have also performed comparison calculations in the nonrelativistic limit, including only lowest-order Doppler and recoil effects, as described by Mészáros and Nagel.[15]

The differential cross sections, normalized to the Thomson cross section and plotted as functions of the final photon energy, are shown in Figs. 1–10. Each figure contains four plots, labeled *A*, *B*, *C*, and *D*, corresponding to scattering from ordinary to ordinary polarization, ordinary to extraordinary, and extraordinary to ordinary, and extraordinary to extraordinary, respectively. The convention used becomes the usual one in the low-frequency limit, where vacuum effects are negligible, namely, transverse ordinary (extraordinary) photons have electric field along (across) the external magnetic field, or longitudinally propagating ordinary (extraordinary) pho-

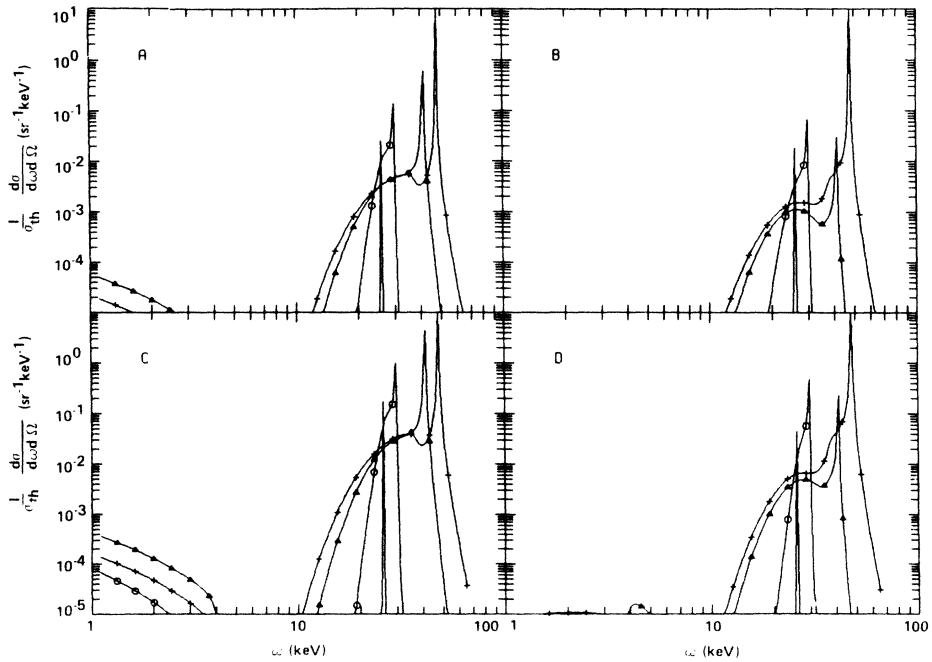

FIG. 1. Relativistic differential scattering cross section (R), incident photon energy 26 keV, and incident angle 15°. The cyclotron energy is 38 keV, the electron longitudinal temperature is 10 keV, and the plasma density is 1.67×10^{-2} g cm^{-3}. Panels *A*, *B*, *C*, and *D* represent *O* to *O*, *O* to *X*, *X* to *O*, *X* to *X*, where *O* and *X* are ordinary and extraordinary polarization. The square, circle, triangle, and cross symbols on the curves denote final photon angles of 20°, 60°, 120°, and 160°, respectively.

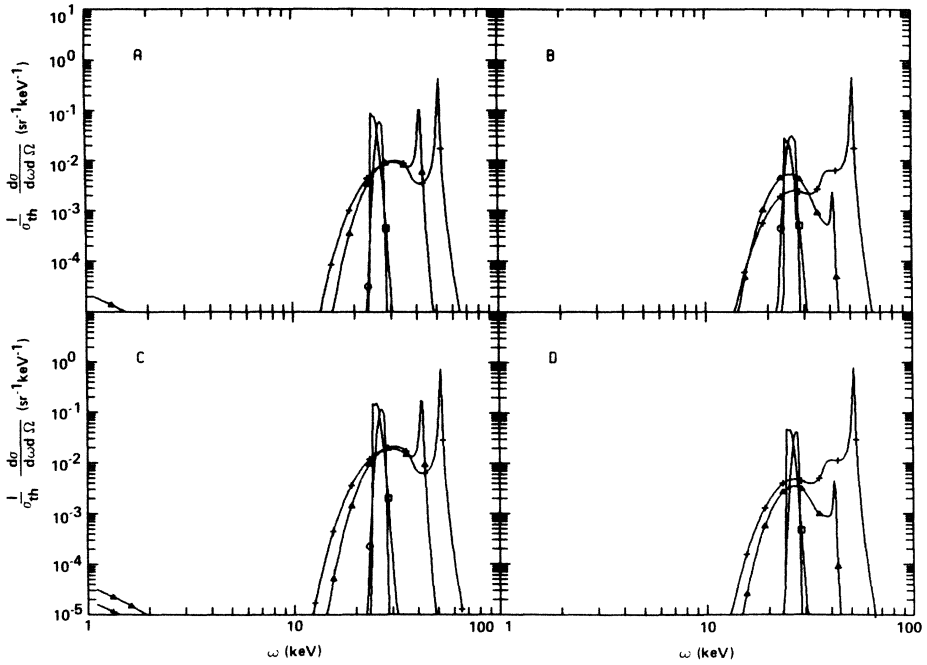

FIG. 2. Same as Fig. 1, incident energy 26 keV, incident angle 45°.

tons have an electric field rotating in the opposite (same) sense as the gyration of an electron in the magnetic field. For a particular incoming photon angle (measured with respect to the magnetic field), the outgoing photon angle is labeled next to the corresponding curve.

Figures 1—3 are the differential cross sections for an incident photon energy of 26 keV and three incident angles: 15°, 45°, and 75°. The plots clearly show the fundamental cyclotron resonance, Doppler shifted according to the final angle, as well as the usual thermal redistribution about the incident frequency. Further, as can be seen by comparing the relativistic case (R) of Fig. 1 with the corresponding nonrelativistic (NR) calculation of Fig. 4, we find a new feature at low energy that corresponds to the production of low-energy photons ($\omega \ll \omega_c$). This effect is caused by a small fraction of the scatterings leaving the electron in an excited state while emitting a low-energy photon. Later the electron radiatively deexcites emitting a

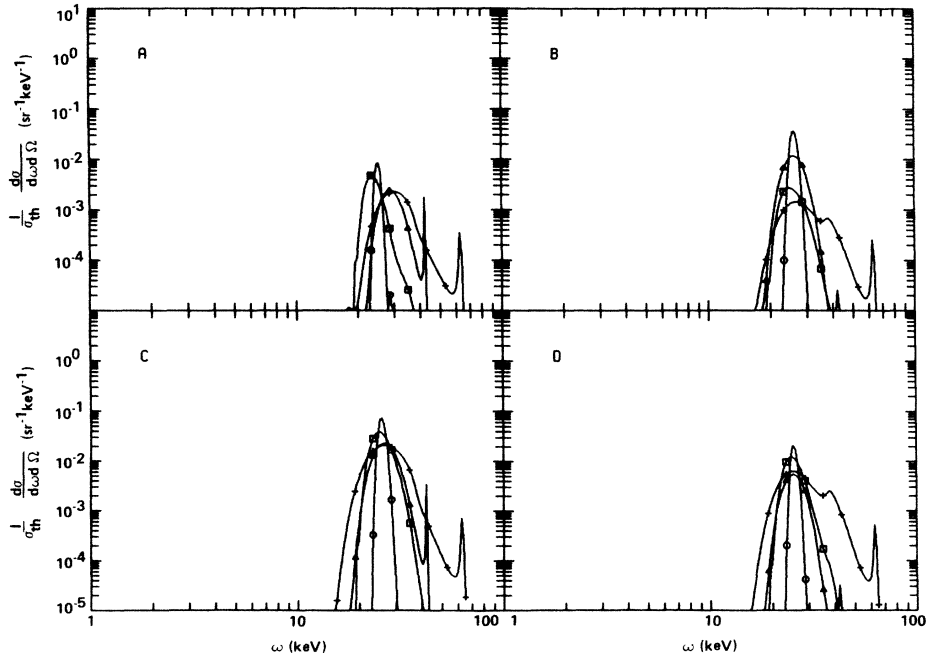

FIG. 3. Same as Fig. 1, incident energy 26 keV, incident angle 75°.

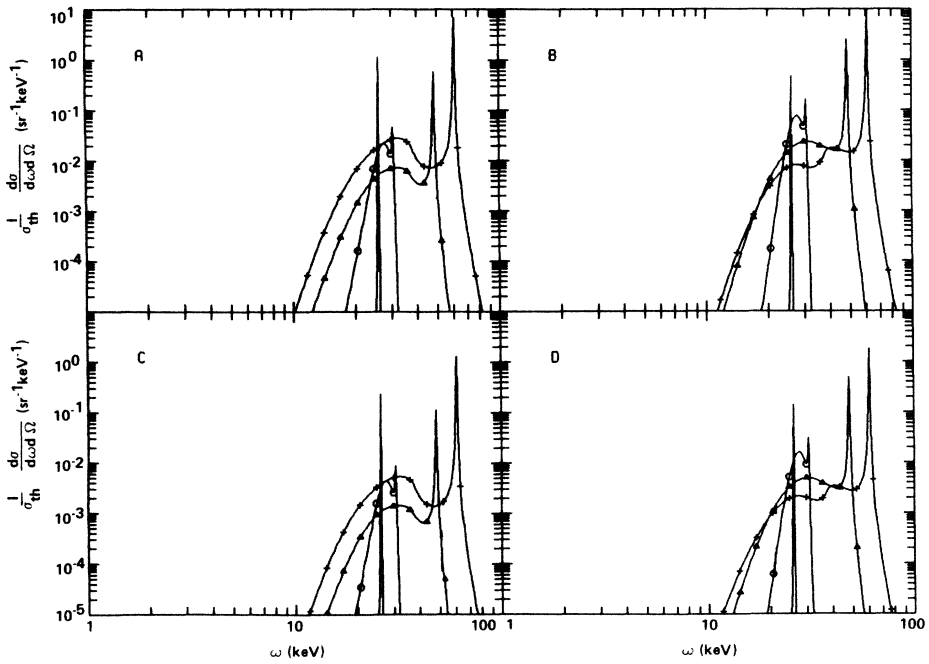

FIG. 4. Same as Fig. 1, but in the nonrelativistic approximation (NR), incident energy 26 keV, incident angle 15°.

resonance photon. The net result is the production of a low-energy or soft photon. In terms of Feynman diagrams, this is analogous to double Compton scattering, which consists of three vertices and two propagators, but in the presence of a strong magnetic field, the second propagator can become a real (on-mass-shell) excited-state electron. A related effect is that of two-photon deexcitation following the absorption of a cyclotron photon. Although we have not included this rate in our calculations, its contribution is nearly equal to that shown at low frequencies in our plots.

The cross sections for an incident photon energy of 50

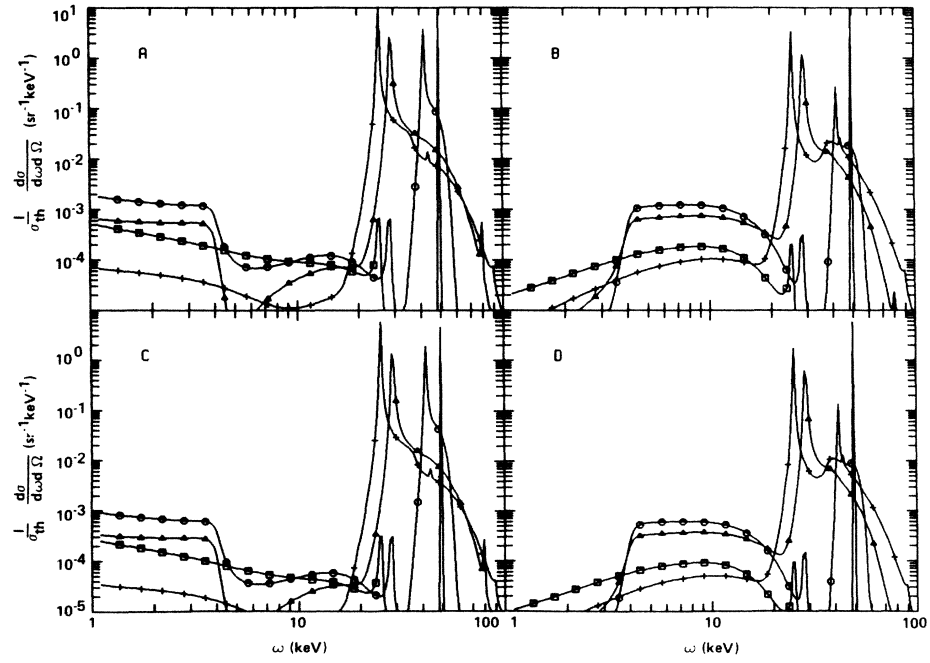

FIG. 5. Relativistic scattering cross section (R), for an incident photon energy of 50 keV, incident angle 15°. Other symbols are the same as in Fig. 1.

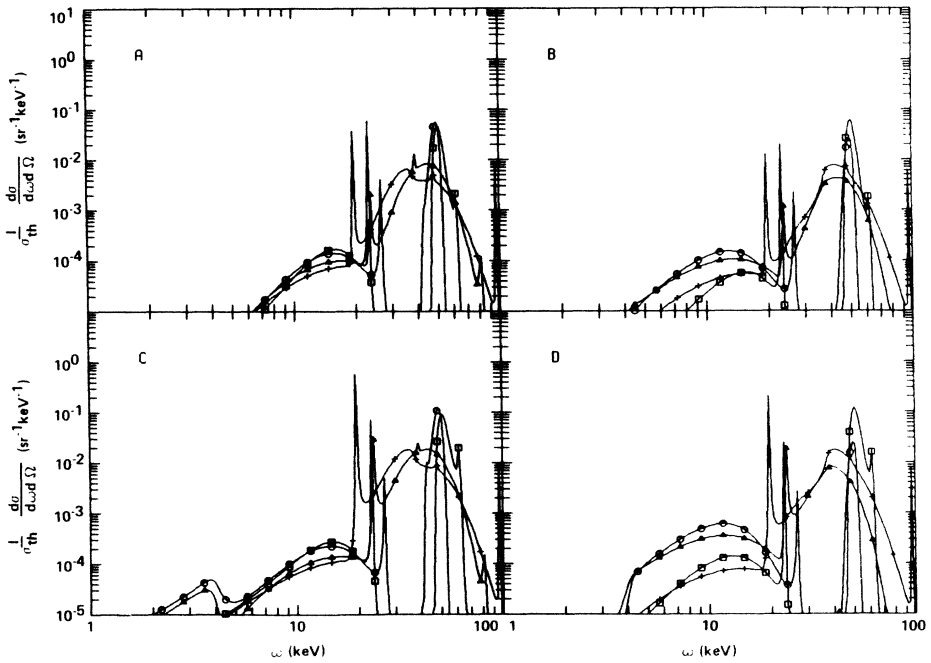

FIG. 6. Same as Fig. 5, incident energy 50 keV, incident angle 45°.

keV are shown in Figs. 5–7. In the relativistic case, we see a large probability for the production of low-energy photons especially at low incident angles. As in the lower-energy case, a nonrelativistic calculation (Fig. 8) contains only the fundamental cyclotron harmonic; whereas the corresponding relativistic one (Fig. 5, as well as Figs. 6 and 7) reveals higher harmonics. This is because an incident photon of 50 keV is sufficient to excite a small fraction of the electrons into the $j=2$ magnetic level. Thus, for example, in Fig. 5, we see not only lines for a $j=1$ to 0 transition but the additional lines corresponding to $j=2$ to 1 and $j=2$ to 0.

As a final example, relativistic calculations were made for the case of an incident photon energy of 100 keV. Here, only two final angles were considered. Figures 9 and 10 show the cross sections for incident angles of 15°

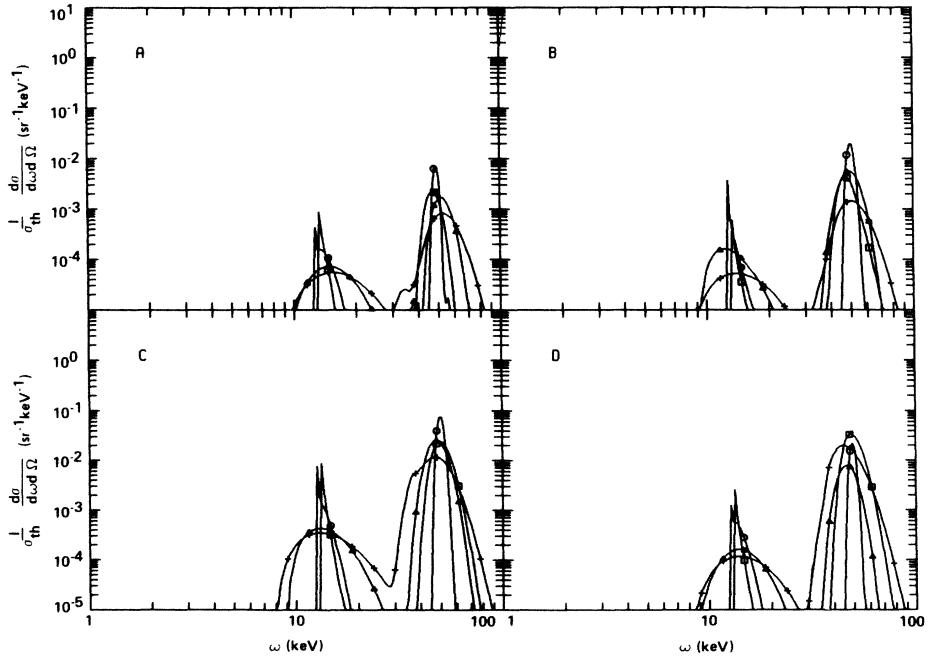

FIG. 7. Same as Fig. 5, incident energy 50 keV, incident angle 75°.

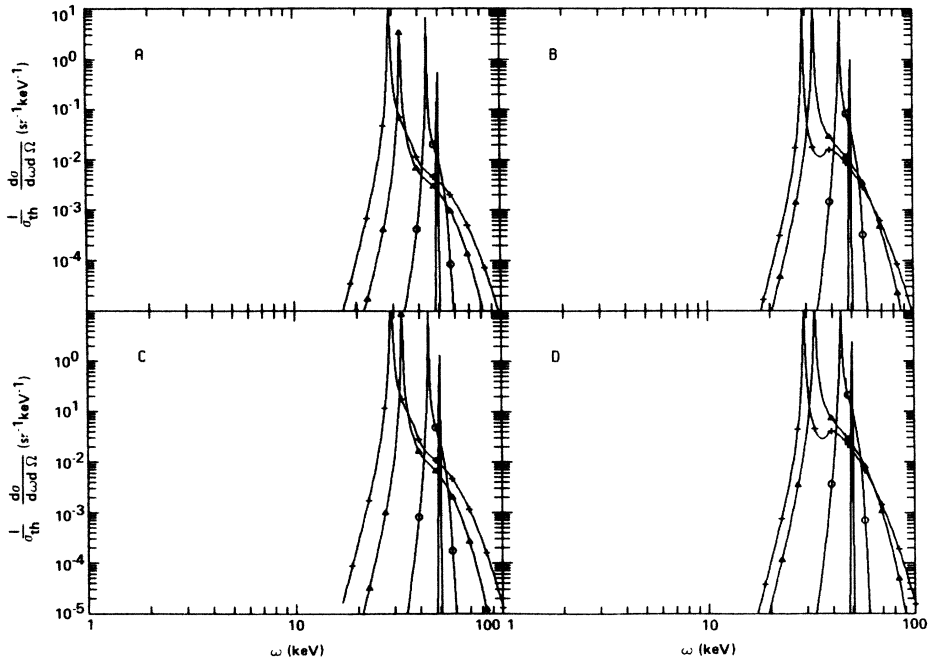

FIG. 8. Same as Fig. 5, but nonrelativistic approximation (NR), incident energy 50 keV, incident angle 15°.

and 75°. Again, the lower final angle shows the probability for the production of soft photons. Also apparent in these figures are the resonances associated with an electron excited to the $j=3$ level.

B. Total scattering cross sections

Total scattering cross sections were computed numerically by integrating the differential cross sections over final photon frequency and solid angle and summing over final polarization. The integration over frequency must be done with special care to ensure that enough frequency points lie close to a resonance. The location of the various resonances is easily calculated from kinematics, and a grid of frequencies is set up that is densest near the resonances and more uniform in the continuum. The total cross sections for ordinary and extraordinary photons, plotted as functions of incident photon frequency for four incident

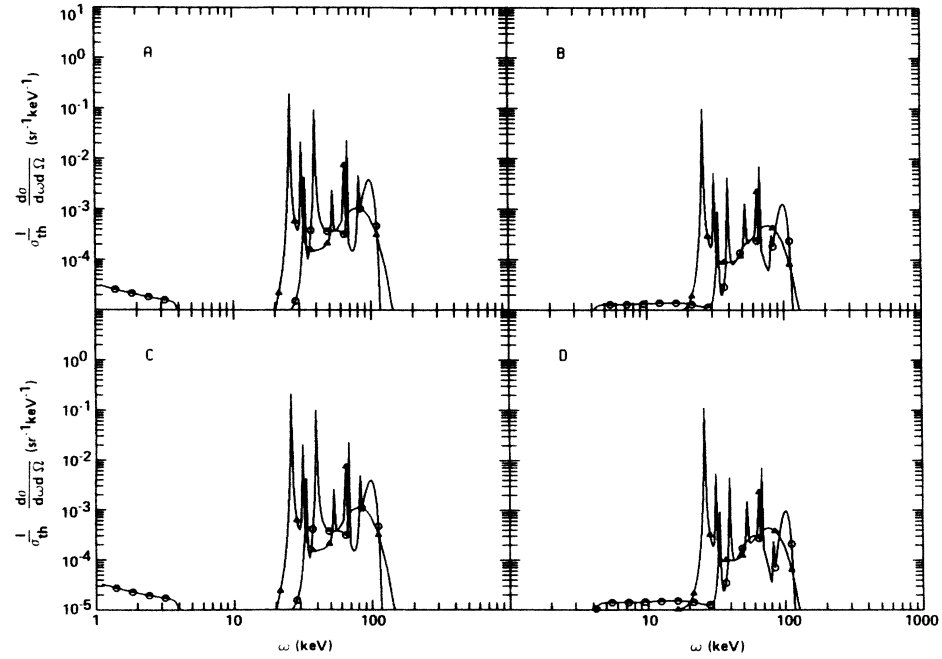

FIG. 9. Relativistic scattering cross section (R) for an incident photon energy of 100 keV, incident angle 15°. Other details are as in Fig. 1.

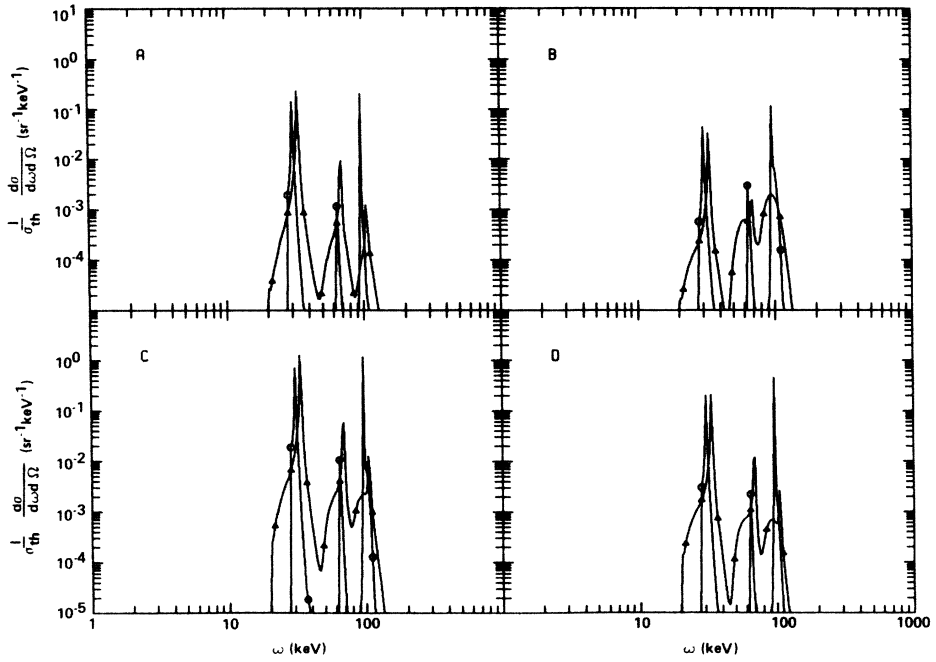

FIG. 10. Same as Fig. 9, incident energy 100 keV, but incident angle 75°.

angles, 15°, 45°, 60°, and 87°, are shown in Figs. 11 and 12 for nonrelativistic and relativistic calculations, respectively. In each case, the cross sections are normalized to the Thomson cross section. At low incident photon energy, the nonrelativistic and relativistic cross sections are virtually identical, including the polarization crossover at the first vacuum frequency,

$$\hbar\omega_V = 3(\rho/0.0167\ \mathrm{g\,cm^{-3}})^{1/2}(B/0.1B_{\mathrm{cr}})^{-1}\mathrm{keV}\ ,$$

as discussed in Ref. 15; this crossover is due to the choice of polarization modes as being given by the medium normal modes, which become degenerate at some particular frequencies, such as at ω_V. At higher energies, the relativistic calculations also show the first and second cyclotron

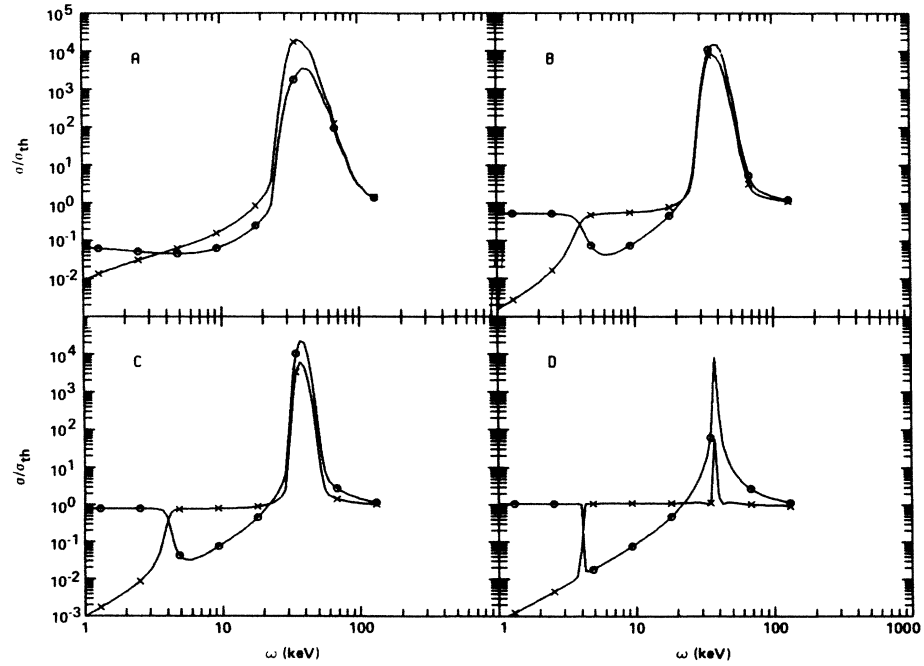

FIG. 11. Nonrelativistic (NR) scattering cross section integrated over final angles and frequencies as a function of the incident energy. The four panels (*A*, *B*, *C*, and *D*) show incident angles of 15°, 45°, 60°, and 87°, respectively. The symbols *O* and *X* on the curves denote ordinary and extraordinary polarizations.

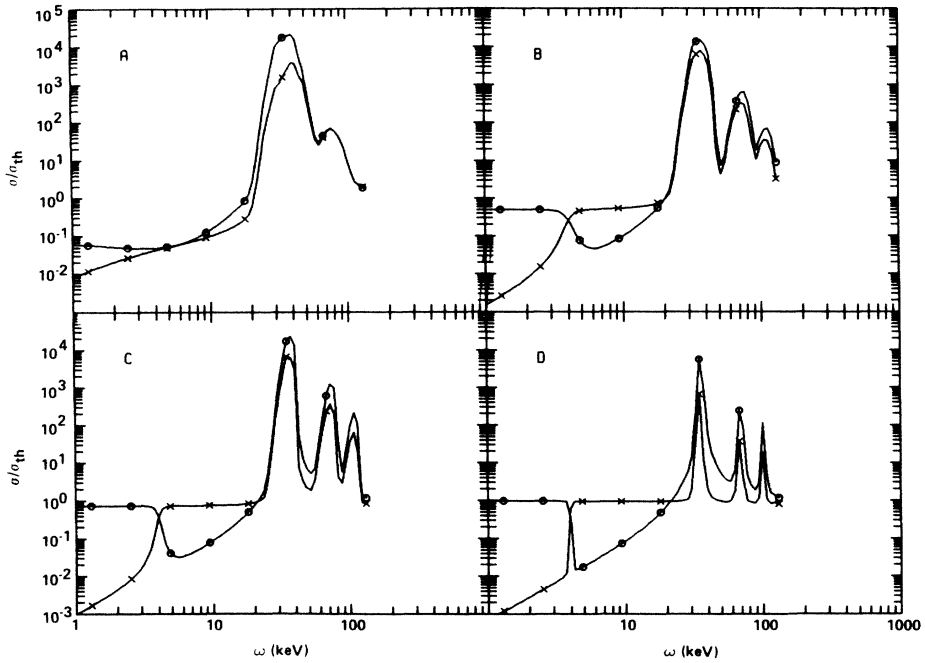

FIG. 12. Same as Fig. 11, relativistic calculation (R).

harmonics at approximately $2\omega_c$ and $3\omega_c$. However, even at the fundamental, there are important differences: In the relativistic case, the peak of the line profile occurs at a lower frequency, and the blue wing falls off more rapidly than in the nonrelativistic calculation.

IV. DISCUSSION

The fully relativistic scattering cross sections for a thermal electron plasma in a strong magnetic field differ noticeably from the values calculated in the nonrelativistic approximation, even for temperatures as low as $\frac{1}{50}$ the electron rest mass, as seen in the preceding section. In the relativistic calculations, the cyclotron resonance peak appears at a lower energy than in the nonrelativistic case, especially for large scattering angles. This is not surprising, since the term describing the anharmonicity of the levels (neglected in the NR case) is actually of similar order of magnitude as the first-order recoil term, which together with the first-order Doppler shift are the only corrections in the NR resonant denominator. The higher-order terms due to recoil also have an effect (cf. Herold, Ruder, and Wunner[16]), while for photon propagation angles close to perpendicular to the field, or $\mu < v/c$, the second-order Doppler shift dominates the first. At electron or photon energies above $\frac{1}{10}$ the electron rest mass, the relativistic expressions become absolutely necessary to avoid significant errors. Even at the modest temperatures of 10 keV as found in many accreting magnetic neutron stars, the frequency half-width over which the scattering redistributes the photons is increased or reduced by about 10—15% in the NR approximation, for photon energies which are 30% below or above the laboratory-frame cyclotron energy. While the relative change is not too important in the case of a single scattering, for photons undergoing multiple scatterings in an optically deep atmosphere this can represent a significant difference in the photon escape time or the resulting line profile.

A new feature introduced in the relativistic calculations presented here is the two-photon scattering, which produces a marked photon production probability at energies below the resonance, for input photons of energy not too different from the resonance energy (e.g., as in these calculations, within about 30% from the resonance). This is in fact the most copious source of photons in accreting x-ray pulsars, easily dominating bremsstrahlung production. Such soft photons, when scattered up in energy by the hotter electrons, can explain the characteristic power-law continuum spectrum detected in these sources (cf. Ref. 8).

The calculations presented here are applicable for calculating the transport of radiation in steady pulsating neutron-star sources, emitting in the x-ray range, and for models of celestial γ-ray burst sources that are based on a neutron-star origin. A relativistic treatment is necessary because of the possible importance of higher harmonics in the high-energy portion of the spectrum, and because of the photon and electron energies in the MeV range for the latter class of objects. Such investigations are underway and will be presented elsewhere. Other areas of application are, e.g., in magnetic fusion and geophysics, where our results can be used in the limit of temperatures comparable to or below the cyclotron ground energy, in the range of frequencies above the electron plasma frequency and above the ion cyclotron frequency.

ACKNOWLEDGMENTS

This research has been partially supported by the National Science Foundation under Grant No. AST 83-13886.

APPENDIX

The derivation of the formulas for the scattering rates consists of calculating the S-matrix element for a given transition and then carrying out the appropriate sums over final states of its square. Labeling the final state f and the initial i, the S-matrix element is

$$S_{fi}=\frac{2\pi}{V}(\omega\omega')^{-1/2}\int d^4x\int d^4x'\bar{\Psi}_f(x)[\hat{\epsilon}'^*\cdot\gamma e^{ik'\cdot x}S(x,x')e^{-ik\cdot x'}\gamma\cdot\hat{\epsilon}+\gamma\cdot\hat{\epsilon}e^{-ik\cdot x}S(x,x')e^{ik'\cdot x'}\hat{\epsilon}'^*\cdot\gamma]\Psi_i(x')\ , \tag{A1}$$

where V is the normalization volume, Ψ represents the electron wave function, k and k' are the four-dimensional wave vectors for the initial and final photon, respectively, ω and ω' are their frequencies, $\hat{\epsilon}$ and $\hat{\epsilon}'$ are the polarization vectors, the components of γ are the Dirac matrices, and $S(x,x')$ is the electron propagator. The wave functions we use are given by

$$\begin{aligned}\Psi(x)&=e^{-iEt}\psi_{nqsp}(\mathbf{x})\ ,\\ \psi_{nqsp}(\mathbf{x})&=\left[\frac{E+m}{2LE}\right]^{1/2}\left[1-\frac{\gamma\cdot\pi}{E+m}\right]f_{nq}(\mathbf{x}_\perp)e^{ipz}u_s\ ,\end{aligned} \tag{A2}$$

where L is a normalization length along the field, the quantum number n is the Landau level (or gyroradius number), s is the spin component along the field, q labels the annulus of the guiding center of the electron orbit, and the continuous variable p is the momentum parallel to the field. The operator π is the canonical momentum, or

$$\pi=\frac{1}{i}\nabla+e\mathbf{A}\ , \tag{A3}$$

where $\mathbf{A}$ is the vector potential of the external field. The spinor u is either (1,0,0,0) or (0,1,0,0) for spin parallel or antiparallel to the field, respectively, and the energy E is given by

$$E=[p^2+2m\omega_c(n+s+\tfrac{1}{2})+m^2]^{1/2}\ , \tag{A4}$$

where ω_c is the classical cyclotron frequency. The functions f_{nq} can be constructed by ladder operators as in Ref. 12. The propagator can be constructed from the spatial parts of the wave functions and an energy denominator, or

$$S(x,x')=\int_{-\infty}^{\infty}\frac{dp_0}{2\pi}e^{-ip_0(t-t')}\times\sum_{\alpha,\lambda}\frac{\psi_\alpha^{(\lambda)}(\mathbf{x})\psi_\alpha^{(\lambda)}(\mathbf{x}')}{p_0-\lambda\left[E_\alpha-\frac{i}{2}\Gamma_\alpha\right]}\ , \tag{A5}$$

where α represents the set of quantum numbers described above and Γ_α denotes the inverse lifetime of the state. The sign of the energy in the solution of the Dirac equation is labeled by λ, and the corresponding negative-energy wave functions are given as in Eqs. (A2) but with basis spinors u replaced by $v=(0,0,1,0)$ or (0,0,0,1). The lifetimes used in this work are determined solely by radiative deexcitations.

After inserting these quantities into the expression for the S matrix, one obtains

$$\begin{aligned}S_{fi}=&\left[\frac{2\pi}{V}\right]^2e^2(\omega\omega')^{-1/2}\delta(E+\omega-E'-\omega')\\ &\times\sum_{\alpha,\lambda}\left[\frac{[\hat{\epsilon}'^*\cdot\mathbf{J}_{f\alpha}^{(\lambda)}(-\mathbf{k}')]\{[\mathbf{J}_{i\alpha}^{(\lambda)}(-\mathbf{k})]^*\cdot\hat{\epsilon}\}}{E+\omega-\lambda\left[E_\alpha-\frac{i}{2}\Gamma_\alpha\right]}+\frac{[\hat{\epsilon}'^*\cdot\mathbf{J}_{\alpha i}^{(\lambda)}(-\mathbf{k}')]\{[\mathbf{J}_{\alpha f}^{(\lambda)}(-\mathbf{k})]^*\cdot\hat{\epsilon}\}}{E-\omega'-\lambda\left[E_\alpha-\frac{i}{2}\Gamma_\alpha\right]}\right]\ .\end{aligned} \tag{A6}$$

Here, the J's represent Fourier transforms of the transition currents, or[12]

$$J_{\alpha\alpha'}^{(\lambda)}(-\mathbf{k})=\frac{2\pi}{L}\left[\frac{E+m}{2E}\frac{E'+m}{2E'}\right]^{1/2}\delta(p+k_{\|}-p')i^{j-j'}(-1)^{q-q'}e^{i(j'-j-q'+q)\phi}F_{qq'}(\xi)G_{\alpha\alpha'}^{(\lambda)}(-\mathbf{k}_\perp)\ , \tag{A7}$$

where $j=n+s+\frac{1}{2}$ is the total magnetic quantum number and ϕ is the photon azimuth in the plane perpendicular to the field. The F functions are given by

$$F_{nn'}(\xi)=i^{|n-n'|}\left[e^{-\xi}\frac{n_<!}{n_>!}\xi^{|n-n'|}\right]^{1/2}L_{n_<}^{|n-n'|}(\xi)\ , \tag{A8}$$

where $n_>$ and $n_<$ are the greater and smaller of n and n', respectively, L represents the associated Laguerre polynomial, and the argument ξ is $k_\perp^2/(2m\omega_c)$. The G functions are given on a spin by spin basis as

$$
\begin{aligned}
[\mathbf{G}^{(+)}_{\alpha\alpha'}(-\mathbf{k}_\perp)]_- &= i\sqrt{2}e^{-i\phi}F_{j,j'-1}(\xi)[\theta_{s,s'}u_\perp+\theta_{-s,-s'}u'_\perp+\theta_{-s,s'}(u'_\parallel-u_\parallel)]\ ,\\
[\mathbf{G}^{(+)}_{\alpha\alpha'}(-\mathbf{k}_\perp)]_+ &= -i\sqrt{2}e^{i\phi}F_{j-1,j'}(\xi)[\theta_{s,s'}u'_\perp+\theta_{-s,-s'}u_\perp+\theta_{s,-s'}(u_\parallel-u'_\parallel)]\ ,\\
[\mathbf{G}^{(+)}_{\alpha\alpha'}(-\mathbf{k}_\perp)]_z &= F_{j-1,j'-1}(\xi)[\theta_{s,s'}(u_\parallel+u'_\parallel)+\theta_{s,-s'}u'_\perp+\theta_{-s,s'}u_\perp]\\
&\quad +F_{j,j'}(\xi)[\theta_{-s,-s'}(u_\parallel+u'_\parallel)-\theta_{s,-s'}u_\perp-\theta_{-s,s'}u'_\perp]\ ,\\
[\mathbf{G}^{(-)}_{\alpha\alpha'}(-\mathbf{k}_\perp)]_- &= i\sqrt{2}e^{-i\phi}F_{j,j'-1}(\xi)[\theta_{-s,s'}(1+u_\parallel u'_\parallel)-\theta_{s,-s'}u_\perp u'_\perp-\theta_{s,s'}u_\perp u'_\parallel+\theta_{-s,-s'}u_\parallel u'_\perp]\ ,\\
[\mathbf{G}^{(-)}_{\alpha\alpha'}(-\mathbf{k}_\perp)]_+ &= -i\sqrt{2}e^{i\phi}F_{j-1,j'}(\xi)[\theta_{s,-s'}(1+u_\parallel u'_\parallel)-\theta_{-s,s'}u_\perp u'_\perp-\theta_{s,s'}u_\parallel u'_\perp+\theta_{-s,-s'}u_\perp u'_\parallel]\ ,\\
[\mathbf{G}^{(-)}_{\alpha\alpha'}(-\mathbf{k}_\perp)]_z &= F_{j-1,j'-1}(\xi)[\theta_{s,s'}(1-u_\parallel u'_\parallel)-\theta_{-s,-s'}u_\perp u'_\perp-\theta_{s,-s'}u_\parallel u'_\perp-\theta_{-s,s'}u_\perp u'_\parallel]\\
&\quad -F_{j,j'}(\xi)[\theta_{-s,-s'}(1-u_\parallel u'_\parallel)-\theta_{s,s'}u_\perp u'_\perp+\theta_{s,-s'}u_\perp u'_\parallel+\theta_{-s,s'}u_\parallel u'_\perp]\ .
\end{aligned}
\tag{A9}
$$

In these expressions,

$$
\begin{aligned}
G_\pm &= \frac{1}{\sqrt{2}}(G_x\pm iG_y)\ ,\\
\theta_{a,b} &= \begin{cases}1 & \text{if } a>0,\ b>0\ ,\\ 0 & \text{otherwise}\ ,\end{cases}\\
u_\perp &= \frac{(2m\omega_c j)^{1/2}}{E+m}\ ,\quad u_\parallel=\frac{P}{E+m}\ ,
\end{aligned}
\tag{A10}
$$

and similarly for the primed quantities. With these definitions, the S-matrix element now becomes

$$
\begin{aligned}
S_{fi} &= \frac{(2\pi)^3}{LV}e^2\left[\frac{E+m}{2\omega E}\frac{E'+m}{2\omega' E'}\right]^{1/2}\delta(E+\omega-E'-\omega')\delta(p+k_\parallel-p'-k'_\parallel)i^{j'-j}(-1)^{q'-q}\\
&\quad\times\sum_{j'',q''}[e^{i(j''-q'')(\phi'-\phi)}e^{-i(j'-q')\phi'}e^{i(j-q)\phi}a_{j''}F_{q'q''}(\xi')F^*_{qq''}(\xi)\\
&\quad\quad +e^{-i(j''-q'')(\phi'-\phi)}e^{i(j-q)\phi'}e^{-i(j'-q')\phi}b_{j''}F_{qq''}(\xi')F^*_{q'q''}(\xi)]\ ,
\end{aligned}
\tag{A11}
$$

where the a's and b's are as defined in the text.

The rate for a given transition is obtained in the usual way by squaring the magnitude of the S-matrix element and multiplying by the appropriate phase-space factors in the final state. The result of this operation can then be averaged over initial guiding center numbers and summed over the final. Without loss of generality, we choose the coordinate system so that the guiding center number of the initial state is zero. To carry out the sum in the final state, we use the relation

$$
\sum_{q''=0}^{\infty}e^{iq''\eta}F_{0q''}(\xi')F^*_{q'q''}(\xi)=i^{q'}(q'!)^{-1/2}(\sqrt{\xi}e^{i\eta}-\sqrt{\xi'})^{q'}\exp\left[-\frac{\xi+\xi'}{2}+\sqrt{\xi\xi'}e^{\eta}\right]\ ,
\tag{A12}
$$

for arbitrary η. The square of the δ functions is handled in the usual way:

$$
\begin{aligned}
|\,\delta(p+k_\parallel-p'-k'_\parallel)\,|^2 &= \frac{L}{2\pi}\delta(p+k_\parallel-p'-k'_\parallel)\ ,\\
|\,\delta(E+\omega-E'-\omega')\,|^2 &= \frac{T}{2\pi}\delta(E+\omega-E'-\omega')\ ,
\end{aligned}
\tag{A13}
$$

where T is a normalization time. Further, the final parallel momentum can be integrated immediately by use of the momentum δ function, yielding

$$
\begin{aligned}
w_{j',s';j,s}(\mathbf{k}',\hat{\boldsymbol{\epsilon}}';\mathbf{k},\hat{\boldsymbol{\epsilon}},\mathbf{p}) &= \frac{e^4}{\omega\omega'}\frac{E+m}{2E}\frac{E'+m}{2E'}\delta(E+\omega-E'-\omega')\left|\sum_{j''}(a_{j''}e^{ij''(\phi'-\phi)}+e^{2i\Lambda}b_{j''}e^{-ij''(\phi'-\phi)})\right|^2\ ,\\
\Lambda &= \frac{j+j'}{2}(\phi'-\phi)+(\xi\xi')^{1/2}\sin(\phi'-\phi)\ ,
\end{aligned}
\tag{A14}
$$

which is identical to Eq. (1) in the text.

[1]P. Joss and S. Rappaport, Ann. Rev. Astron. Astrophys. **22**, 537 (1984).
[2]P. Mészáros, Space Sci. Rev. **38**, 325 (1984).
[3]V. Canuto, J. Lodenquai, and M. Ruderman, Phys. Rev. D **3**, 2303 (1971).
[4]J. Ventura, Phys. Rev. D **19**, 1684 (1979).
[5]P. Mészáros and J. Ventura, Phys. Rev. D **19**, 3565 (1979).
[6]J. K. Daugherty and J. Ventura, Phys. Rev. D **18**, 1053 (1978).
[7]H. Herold, Phys. Rev. D **19**, 2868 (1979).
[8]R. W. Bussard, P. Mészáros, and S. Alexander, Astrophys. J. Lett. **297**, L21 (1985).
[9]J. G. Kirk and D. B. Melrose, Astron. Astrophys. (to be published).
[10]J. D. Bjorken and S. D. Drell, *Relativistic Quantum Mechanics* (McGraw-Hill, New York, 1964).
[11]V. Canuto and J. Ventura, Fund. Cosmic Phys. **2**, 203 (1977).
[12]R. W. Bussard, Astrophys. J. **237**, 870 (1980).
[13]R. W. Bussard, F. K. Lamb, and D. Pakey, Marshall Space Flight Center Report No. 86-130, 1986 (unpublished).
[14]G. G. Pavlov, Yu. A. Shibanov, and D. G. Yakovlev, Astrophys. Space Sci. **73**, 33 (1980).
[15]P. Mészáros and W. Nagel, Astrophys. J. **298**, 147 (1985).
[16]H. Herold, H. Ruder, and G. Wunner, Plasma Phys. **23**, 775 (1981).